NANO LETTERS

pubs.acs.org/NanoLett

Letter

Skin-Inspired Self-Aligned Silicon Nanowire Thermoreceptors for Rapid and Continuous Temperature Monitoring

Zongguang Liu, Rongrong Yuan, Shuyi Wang, Wei Liao, Lei Yan, Ruijin Hu, Jianmei Chen,* and Linwei Yu*

Cite This: *Nano Lett.* 2025, 25, 4196−4203

Read Online

ACCESS | Metrics & More | Article Recommendations | Supporting Information

ABSTRACT: Real-time and precise evaluation of human body temperature offers crucial insights for health monitoring and disease diagnosis, while integration of high-performance and miniaturized sensors remains a challenge. Inspired by the thermal sensory pathway of skin, here we developed a new route for scalable fabrication of rapid-response and miniaturized thermoreceptor sensors using self-aligned in-plane silicon nanowire (SiNW) arrays as sensitive channels. These SiNW arrays, with a diameter of 100 ± 14 nm, were integrated into temperature sensors with a density of 445 devices/cm^2 without using any high-precision lithography. The sensors exhibited an excellent temperature coefficient of resistance of −1.8%/°C, enabling the precise spatial identification of heat sources. They achieved real-time monitoring of temperature changes during breathing and blowing activities, with a rapid response time of ∼0.2 s and recovery time of ∼1 s. This study provides a robust foundation for the integration of advanced miniaturized temperature sensors for biological monitoring applications.

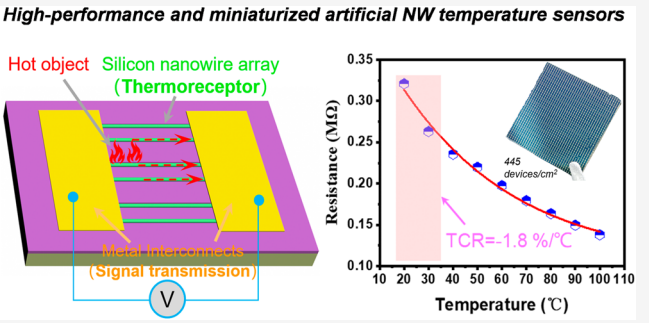

KEYWORDS: *In-plane SiNW integration, Miniaturized temperature sensor, Ohmic contact, Annealing process, Surface defects*

Body temperature serves as a pivotal metric for monitoring human activities and health status, often acting as an auxiliary diagnostic tool for conditions such as cardiovascular disease, pulmonary diagnostics, and intestinal infections.[1,2] Continuous and real-time monitoring of body temperature, by comparison of patient-recorded data with standard curves, can facilitate early disease screening and clinical diagnosis. For instance, fever is a typical clinical symptom of both influenza and the global Coronavirus Disease 2019 (COVID-19),[3,4] with a slight increase in body temperature serving as a straightforward initial indicator of potential infection. Unfortunately, traditional body temperature detection methods, like mercury or infrared thermometers, are limited to single-point measurements rather than providing long-term continuous monitoring.[5]

Recently, a variety of inorganic and organic heat-sensitive materials, including carbon materials (reduced graphene oxide,[5,6] carbon nanotubes[7]), NiO film,[8] polyaniline,[9] silver nanowire films,[10−13] poly(3,4-ethylenedioxythiophene):polystyrene (PEDOT:PSS),[14−16] and ionic conductive hydrogels,[17−19] have been extensively studied as core components for real-time temperature-monitoring sensors. However, the developed sensor devices are fairly big in size and lack high sensitivity, presenting challenges for device integration and achieving high spatial resolution. Consequently, recent efforts have concentrated on developing thermoreceptors with miniature distributed sensors that offer excellent sensitivity, rapid response times, and stable, precise reactions to temperature changes.

The biological thermal sensory neural pathway present in human skin provides a smart model for continuous, high-resolution monitoring of body temperature. As depicted in Figure 1a, this pathway mainly comprises spatially distributed thermoreceptors and a signal transmission system. External thermal stimuli are detected and converted into electrical signals (action potentials) by thermoreceptors, which are subsequently relayed to the brain via the nervous system. Under the processing and instruction of the brain, the human body perceives and responds to the external stimuli.[1] Specifically, to mimic the miniaturized and distributed architecture of biological thermoreceptors on skin, large-area aligned ultrathin sensitive materials are required. Although the artificial sensor has been developed using the aligned thermosensitive V_2O_5 nanowires (NWs) as the sensitive materials,[20] their complex fabrication processes and dense

Received: October 22, 2024
Revised: February 27, 2025
Accepted: February 28, 2025
Published: March 10, 2025

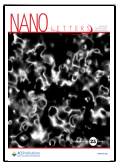

https://doi.org/10.1021/acs.nanolett.4c05235
Nano Lett. 2025, 25, 4196−4203

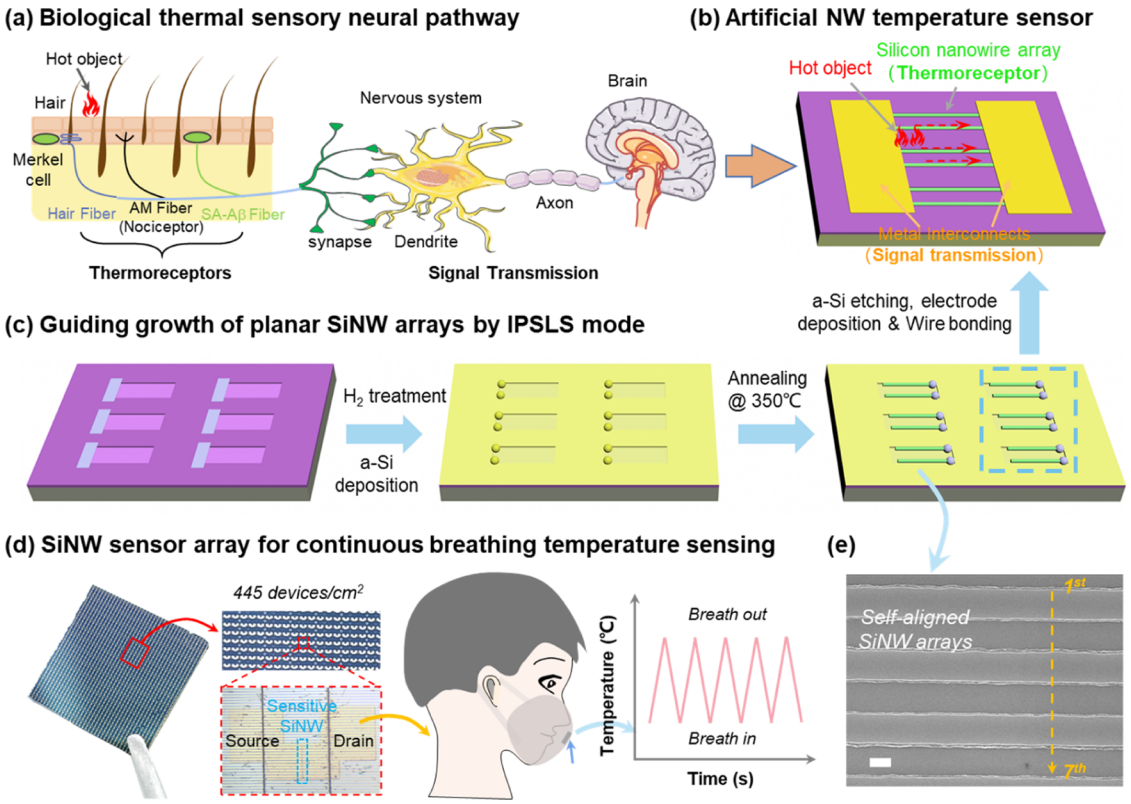

Figure 1. (a) Schematic diagram of thermal sensing and signal transmission on human skin. (b) Artificial temperature sensors fabricated using aligned SiNW arrays. (c) Growth integration of self-positioned SiNW sensor channels via the IPSLS mode. (d) Scalable and minimalized SiNW sensors for continuous temperature monitoring. (e) SEM image of the as-grown SiNW arrays. Scale bar in (e) stands for 2 μm.

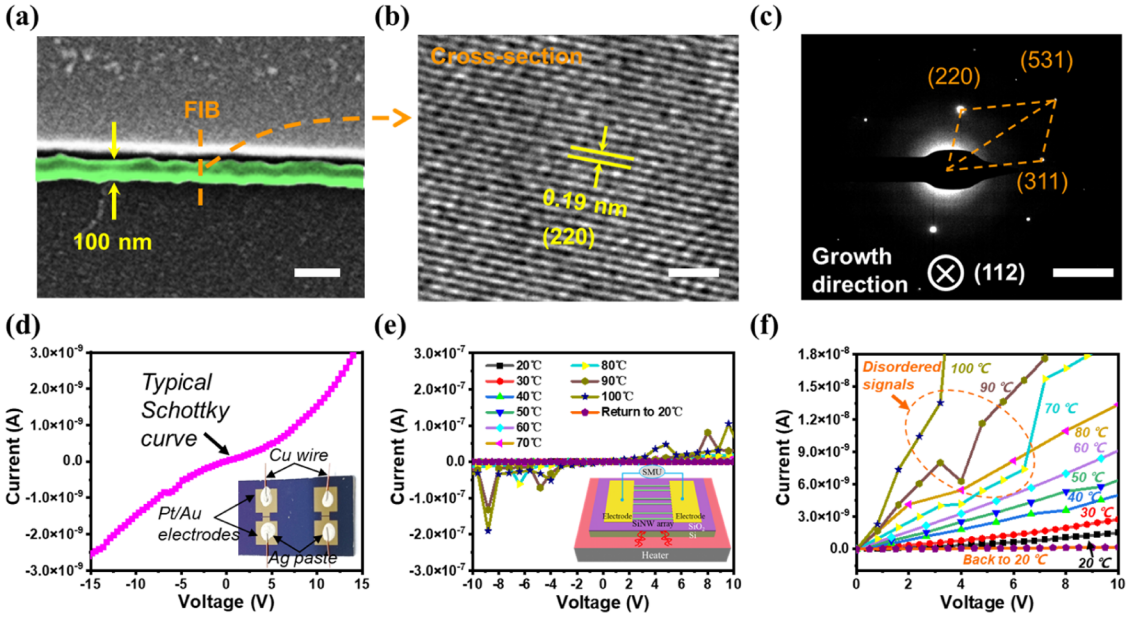

Figure 2. (a) Typical SEM image of the as-grown IPSLS SiNW. (b) HRTEM image of the cross-section of a selected SiNW in (a), along with the corresponding electron diffraction pattern shown in (c). (d) Current−voltage curve of the fabricated two-terminal sensor device, with the device photograph included as an inset. (e) Current−voltage curves of the sensor device under various temperature conditions, with the enlarged curves provided in (f). The inset in (e) shows the schematic diagram of the temperature detection by the SiNW sensor. The scale bars in (a), (b), and (c) are 100 nm, 1 nm, and 5 nm^{-1}, respectively.

NW clusters require further optimization for the integration of high-density, miniaturized sensor electronics.

In this work, we have developed a large-area, high-performance artificial thermoreceptor inspired by the thermal sensory neural pathways in the skin, fabricated by self-aligned silicon nanowire (SiNW) arrays grown via an in-plane solid−liquid−solid (IPSLS) strategy established in our previous works.[21−25] Unlike the conventional vapor−liquid−solid

https://doi.org/10.1021/acs.nanolett.4c05235
Nano Lett. 2025, 25, 4196−4203

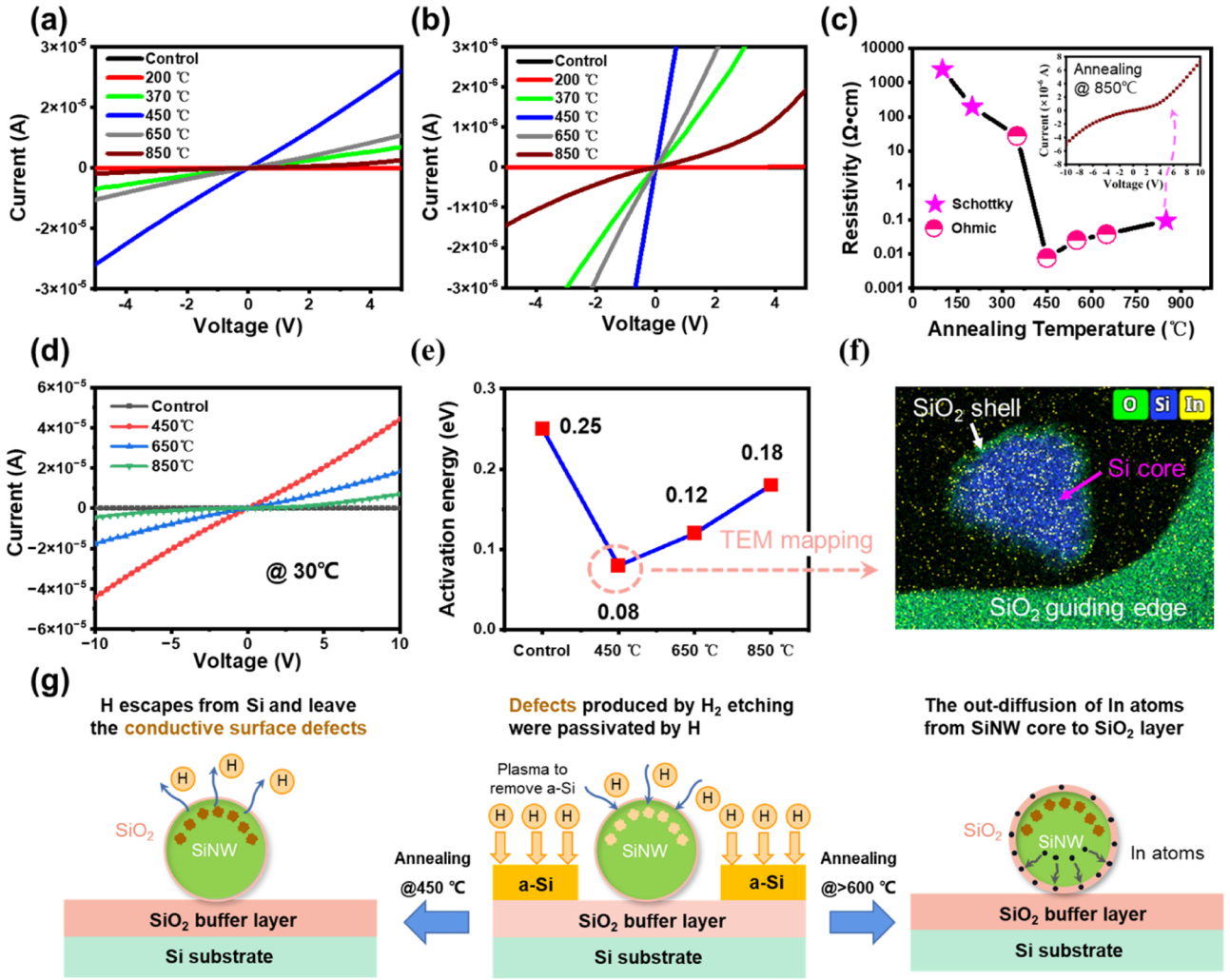

Figure 3. (a) Current−voltage curves of devices fabricated by SiNW channels annealed at various temperatures; the enlarged curves are shown in (b). (c) Calculated resistivity of the SiNWs as a function of typical annealing temperature. (d) Current−voltage curves of the SiNW device measured at a set temperature of 30 °C after annealing at different temperatures. (e) Activating energy calculated for the SiNWs following annealing treatment. (f) TEM elemental mapping image of the cross-section of the SiNW channel after annealing at 450 °C. (g) Schematic representation of the surface states of the SiNWs at different annealing temperatures.

(VLS) growth method, which uses gaseous precursors and tends to produce vertically aligned SiNW bundles, the IPSLS approach employs an amorphous silicon (a-Si) film to supply solid precursors for SiNW growth on the substrate surface. Indium (In) catalyst droplets were used to absorb the a-Si layer and move along predefined edges to create well-aligned planar crystalline SiNW arrays, which facilitates the scalable integration of electronic devices.[26−29] The SiNW channels used here are the most mature and stable semiconductors, which possess high temperature sensitivity, making them ideal candidates for constructing high-performance sensors. Similar to bulk silicon, the temperature sensing capability of SiNWs stems from changes in carrier concentration and mobility with temperature.[30−32] As shown in Figure 1b, the artificial temperature sensors consist of two parts: the self-aligned IPSLS SiNWs serve as the heat-sensitive thermoreceptor layer, while the two metal electrodes prepared by photolithography and metal deposition were used as interconnectors for signal transmission. Upon receiving a thermal stimulus, the thermoreceptors perceive and convert it into an electrical signal, which is then transmitted to the detection device.

The aligned SiNW array was grown on a SiO_2/silicon wafer substrate via an IPSLS guided growth strategy, led by the In catalyst droplets, as illustrated in Figure 1c. The detailed process is presented in the Experimental Section in the Supporting Information (SI). The typical SEM image of the as-grown 7-layer SiNW array along the guiding edges is shown in Figure 1e, with an average diameter of D_{NW} = 100 ± 14 nm, as witnessed in Figure S1. Thanks to the guiding growth of the self-aligned in-plane SiNW array, large-area and high-density SiNW sensors (445/cm^2) were readily mass-produced using a conventional photolithography technology, as shown in the left panel in Figure 1d. Note that the integration density of the sensor devices can be further increased by reducing the sizes of metal electrodes. These SiNW sensors can find applications in biology, such as continuously monitoring temperature variations during body breathing activity (right panel in Figure 1d).

The crystallinity of the selected SiNWs (Figure 2a) was examined using high-resolution transmission electron microscopy (HRTEM). The cross-sectional slice of the SiNW was prepared by focused ion beam milling. The coherent crystalline

https://doi.org/10.1021/acs.nanolett.4c05235
Nano Lett. 2025, 25, 4196−4203

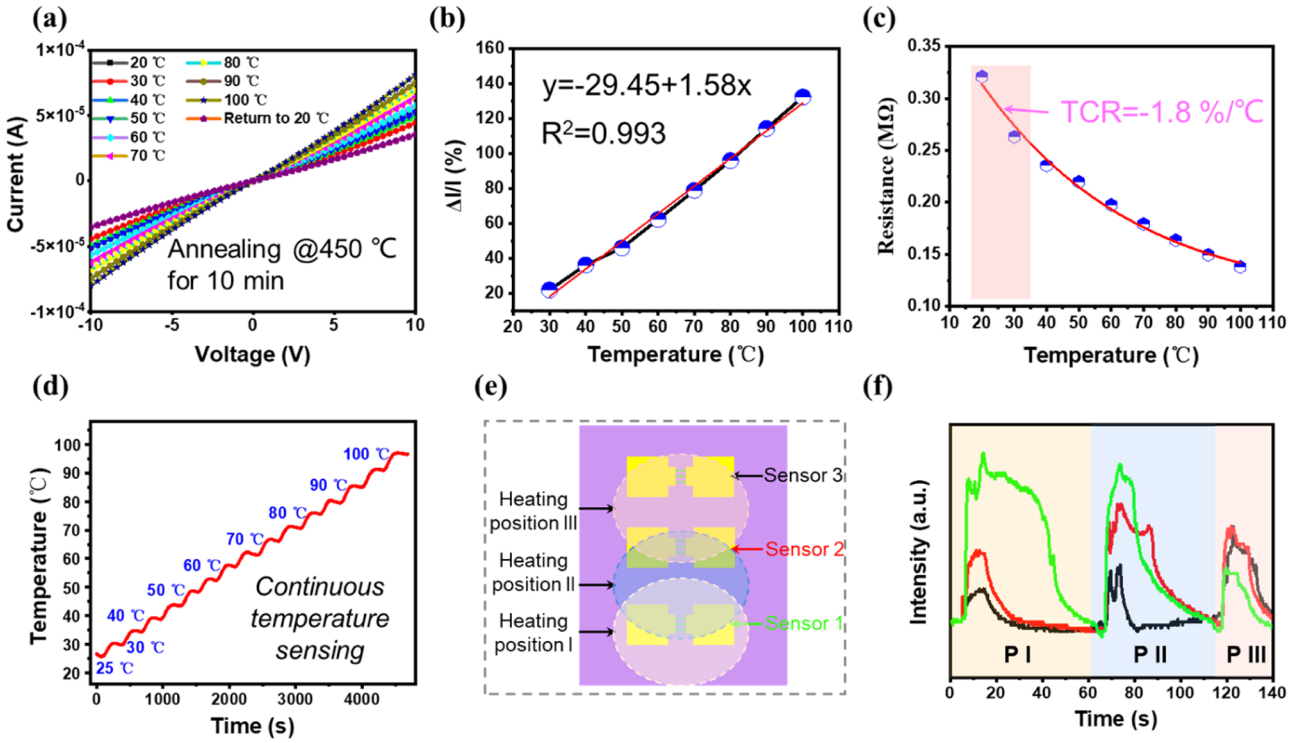

Figure 4. (a) Current−voltage curves of the sensors fabricated using the SiNW channels after being annealed at 450 °C, measured at different heating temperatures. (b) Corresponding $\Delta I/I_0$ versus temperature curve under a 2 V bias. (c) Calculated resistance curve varying with temperature, with the TCR of −1.8%/°C. (d) Continuous sensing performance of the device over a temperature range of 25 to 100 °C, with increments of 5 °C. (e) Schematic diagram illustrating the spatially resolved application of the sensor using heated gas at different positions; (f) the corresponding response curves.

lattice exhibits a clear fringe spacing of d = 0.19 nm (Figure 2b), corresponding to Si ⟨220⟩ planes. According to the electron diffraction pattern shown in Figure 2c, a preferential growth orientation of Si ⟨112⟩ can be observed.

In the fabrication of standard two-terminal SiNW sensors, platinum/gold (Pt/Au) electrodes were patterned and deposited at the two ends of the SiNWs. Subsequently, silver (Ag) paste was employed to bond these electrodes to external testing equipment using copper (Cu) wires, as depicted in the inset photo in Figure 2d. The current−voltage curve of the fabricated sensor device indicates that the as-grown SiNWs formed a pair of typical back-to-back Schottky barrier (SB) junctions when contacted with the Pt/Au electrode, which is consistent with our previous findings.[33] This was attributed to the fact that the dissolution of In atoms into the SiNWs results in p-type doping, equivalent to a boron doping concentration of 5×10^{18} cm^{-3}.[34]

To evaluate the temperature sensing capability of the SiNW sensors, we established a series of temperatures ranging from 20 to 100 °C using an electrically controlled heater. When the sensor was placed on the heater, heat was transferred to the sensor, and the current−voltage (I−V) curves at different temperature states were measured by using a source meter (inset in Figure 2e). Figures 2e and 2f demonstrate that the detected current flowing through the SiNW channels increased with rising temperature. This phenomenon can be explained by the changes in carrier concentration and mobility with temperature.[30] Unfortunately, the SB junction and the resultant discordant signals from the sensors lead to nonlinear responses to temperature variations, making them challenging and complex for high-precision temperature sensing applications.

In general, the annealing process has been proven to be an effective way to improve the contact quality of semiconductors and metals. Inspired by previous knowledge, we attempted to anneal the as-grown SiNWs under a low-vacuum condition (∼5 Pa) at different temperatures ranging from 200 to 850 °C for 10 min in a furnace. Figure 3a shows the room temperature (20 °C) current−voltage curves of fabricated devices using SiNW channels annealed at these different temperatures. At a relatively low temperature (200 °C), there was negligible improvement in the contact characteristics (still Schottky) and current (red line) compared to the control sample (black line, without annealing). When the annealing temperature was raised up to 370 °C, the SiNW−metal contact transitioned to typical Ohmic contact mode (linear current−voltage curve), as shown in the enlarged curves in Figure 3b. The measured current reached its maximum value at 450 °C, while the current decreased when using the annealing temperatures of 650 and 850 °C. These results can also be demonstrated by the results of extracted resistivity values of the annealed SiNW channels, as witnessed in Figure 3c. Compared to the unannealed SiNWs, the resistivity of the SiNW annealed at 450 °C decreased by more than 5 orders of magnitude. The uniformity of the fabricated devices is evidenced by the consistent current−voltage characteristics observed across 20 samples (Figure S2). Notably, despite their high conductivity, the SiNWs retain semiconducting properties and exhibit significant sensitivity to visible light illumination (Figure S3). In addition, it was observed that the metal contacts to SiNWs annealed between 370 and 650 °C exhibited Ohmic behavior,

https://doi.org/10.1021/acs.nanolett.4c05235
Nano Lett. 2025, 25, 4196−4203

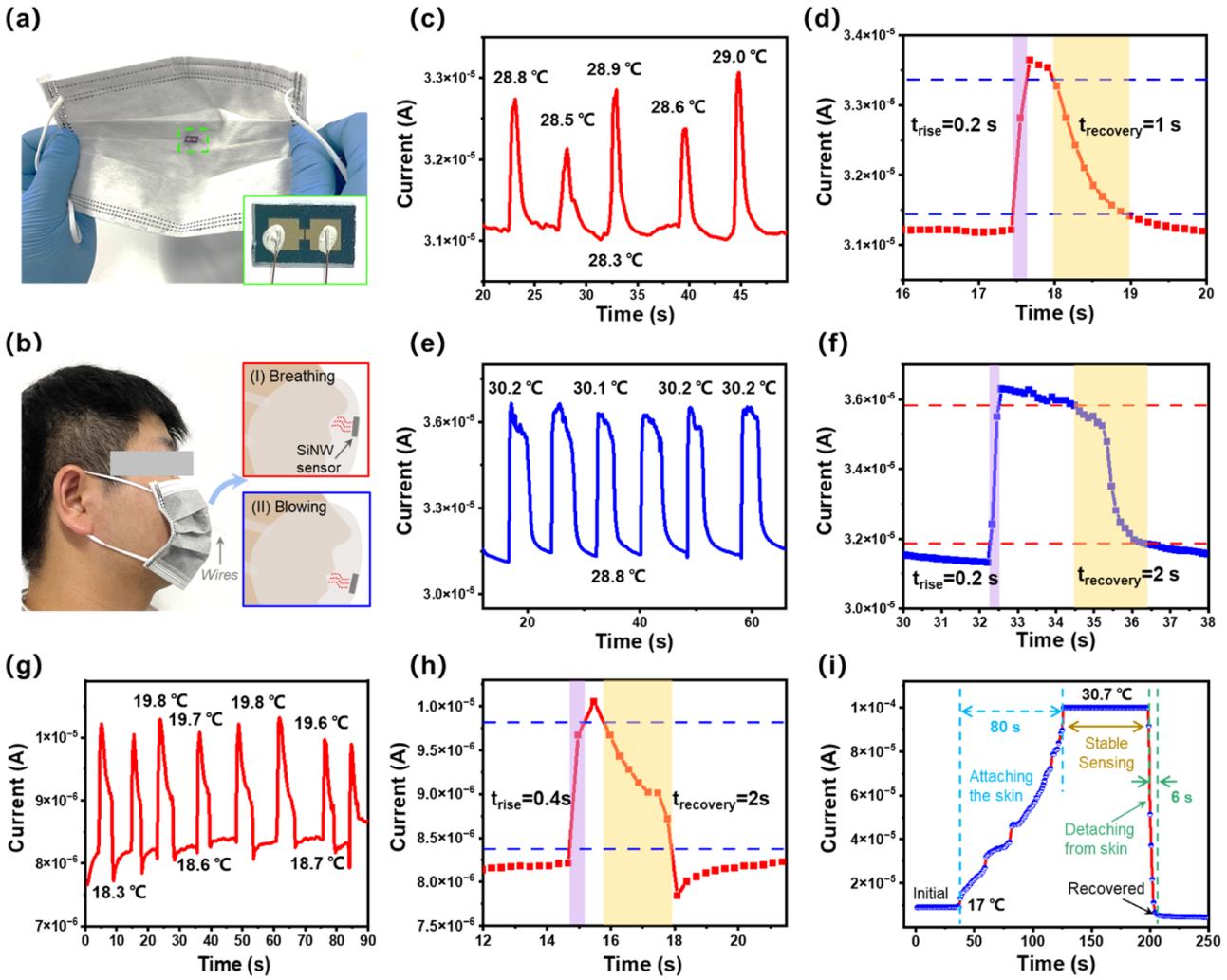

Figure 5. (a, b) Photos of the SiNW sensor integrated into a face mask, demonstrating its application in monitoring breathing and blowing activities. (c) Continuous sensing of breathing temperature from the nose; (d) the extracted response times (t_{rise} and $t_{recovery}$). (e) Temperature sensing response to blowing from the mouth; (f) extracted response times. (g, h) Continuous sensing of breathing temperature through the nose and the corresponding extracted response times at a relatively low ambient temperature of ~18 °C. (i) SiNW sensor for continuous skin temperature monitoring.

whereas those annealed at 850 °C reverted to Schottky behavior, similar to the control sample.

Despite high-temperature annealing at 650 and 850 °C leading to increased resistance in Ohmic contacts or even forming Schottky contacts with metal electrodes, the fabricated sensors maintained their temperature-sensitive performance across a range from 20 to 100 °C, as shown in Figure S4. We further extracted the current−voltage curves of these sensors upon exposure to a 30 °C environment. The results indicated that the sensor fabricated from SiNW channels annealed at 450 °C showed the highest response current (red line) compared to the control sample and sensors annealed at 650 and 850 °C, as depicted in Figure 3d. To understand this interesting observation, we calculated the activation energy (E_a) of the SiNW annealed at the aforementioned temperatures through the equations in the SI. E_a represents the minimum amount of energy required to initiate a reaction, implying that SiNW materials with a lower E_a exhibit a higher sensitivity to temperature changes. The dependence of $\ln(1/R)$ on $1/kT$ is shown in Figure S5, where the slope of the line corresponds to the E_a of SiNWs. The results presented in Figure 3e show that the SiNWs annealed at 450 °C exhibited the lowest E_a value of 0.08 eV, while the unannealed SiNWs and those annealed at 650 and 850 °C had E_a values of 0.25, 0.12, and 0.18 eV, respectively.

The elemental mapping images of a FIB etched cross-sectional slice of SiNW annealed at 450 °C were obtained by using a field emission transmission electron microscope (TEM), as shown in Figure 3f and Figure S6. The results indicate that the In atoms are uniformly distributed within the SiNW core, suggesting that the annealing process at this temperature level has a negligible effect on the redistribution of doped In and the Fermi level. Therefore, we suggested that the change from the initial Schottky contact to an Ohmic contact after annealing at 450 °C can be attributed to the modification in the surface state, as schematically depicted in Figure 3g. At the end of IPSLS growth, hydrogen plasma etching removes the residual a-Si layer around the SiNWs, causing their sidewall damage, including dangling bonds or surface defects. Meanwhile, the small hydrogen atom can also passivate these surface defects during the etching process, resulting in an initial Schottky contact (middle panel in Figure 3g). When the

https://doi.org/10.1021/acs.nanolett.4c05235
Nano Lett. 2025, 25, 4196−4203

SiNWs were annealed at 450 °C, the hydrogen atoms escaped from the SiNWs (left panel in Figure 3g), leaving behind the highly conductive defects and improving the conductivity and contact mode to metal electrodes. When the annealing temperature reached above 600 °C, the segregation of dissolved In atoms at the Si/SiO_2 interface facilitated the extraction of In atoms from the SiNW cores into the outer SiO_2 shell,[34] resulting in the decrease of conductivity, as shown in the right panel in Figure 3g. Upon further elevation of the temperature to 850 °C, the enhanced segregation process further reduced the In doping concentration and conductivity of SiNWs, ultimately reverting the contact to a Schottky mode.

Thanks to the low-resistance Ohmic contact between the annealed SiNWs (at 450 °C) and the Pt/Au electrodes, the detected current flowing through these SiNW channels uniformly increased as the temperature rose from 20 °C to 100 °C (Figure 4a). To quantify the thermal sensitivity, we further extracted the current values from the curves under a voltage bias of 2 V and calculated the relative change in the current ($\Delta I/I_0 = (I - I_0)/I_0$), where I and I_0 are the currents at the measured temperature and initial temperature (i.e., 20 °C), respectively. As shown in Figure 4b, $\Delta I/I_0$ increased linearly with the rising temperature, achieving an R^2 value of 0.993, which is indicative of the typical negative temperature coefficient of resistance (TCR) characteristic of silicon materials.[31,35] The TCR is a key metric for evaluating the thermal response of temperature sensors, representing the rate of resistance change per degree of temperature variation. The TCR value of the sensor is defined as $\mathrm{TCR}\,(\%) = \frac{\Delta R}{R_0 \cdot \Delta T} \times 100\%$, where R_0 is the initial resistance value of the SiNW and ΔR is the change in resistance corresponding to the temperature change ΔT.[36] Specifically, the TCR of the SiNW temperature sensor was calculated to be excellent, −1.8%/°C, over the temperature range of 20−35 °C (Figure 4c), which is suitable for the biological breathing temperature sensing applications. Although the TCR value of these SiNW array sensors was lower than that reported for SiNW fabric sensors synthesized via the chemical vapor deposition VLS method (TCR = 7.71%/°C),[31] the unique self-aligned in-plane structure of the SiNW arrays provides a high capability for the integration of high-performance miniaturized and distributed sensors over a large area, which has never been demonstrated before.

The results in Figure 4d show that the device exhibits continuous sensing performance across a temperature range from 25 to 100 °C, with increments of 5 °C. We further investigated the spatially resolved temperature sensing ability of the SiNW sensors by applying heated gas to different positions. The heating position was controlled by moving the tube tip, as illustrated in the three circles depicted in Figure 4e. When the hot gas was directed to position I, the entire sensing area (the region between the two electrodes containing the SiNW channels) of sensor I was covered, while the other two sensors remained unaffected. Consequently, a significant increase in signal intensity due to the temperature increase was observed in sensor I (green curve), as shown in Figure 4f. All signals returned to their initial state when the hot gas was removed. It is worth noting that the small signal intensities in sensors II (red curve) and III (black curve) can be attributed to the heat transfer process on the SiO_2/Si substrate during the measurement. These effects could be minimized using a smaller heat source. Similar responses were observed when the hot gas was delivered to positions II and III. This real-time temperature mapping opens up numerous advanced applications, such as artificial electronic skins and the detection of emotional changes.

To evaluate the continuous sensing capability of the SiNW sensors for detecting breathing and blowing temperatures, the sensors were mounted on the interior surface of face masks, positioned approximately 2 cm from the nose and mouth, as shown in the optical images in Figures 5a and 5b. A voltage bias was applied to the devices, and the resulting current variations were measured via the tiny Cu wires that traversed the masks. When exhaling hot air, the temperature around the sensor increases, leading to a noticeable rise in the current signal due to the decreased resistance of the sensitive SiNW materials. The current will recover to the initial value when air is breathed in. The detected current signals were converted into temperature values based on the current−temperature curve shown in Figure 4b, yielding an average temperature (T_{avg}) of 28.8 ± 0.26 °C (Figure 5c). The measured temperature is slightly lower than the average exhaled breath temperature of healthy individuals (~34 °C),[37] which can be attributed to heat loss during measurement. This discrepancy can be easily calibrated for clinical monitoring applications. The response times for sensing temperature were further extracted from Figure 5c, showing that the sensor rapidly responds to temperature variations, with a rise time of 0.2 s and a recovery time of 1 s (Figure 5d). Similarly, the sensor responded to blowing temperature variations, with an average detected temperature of T_{avg} = 30.2 ± 0.28 °C (Figure 5e), a rise time of 0.2 s, and a recovery time of 2 s (Figure 5f). Additionally, the sensing performance and response times of the sensors at a relatively low ambient temperature (~18 °C) yielded results similar to those in Figures 5c and 5d (ambient temperature ~28 °C), with a detected temperature of ~19.7 °C, a rise time of 0.4 s, and a recovery time of 2 s (Figures 5g and 5h), demonstrating their excellent environmental adaptability. Compared to a commercial sensor (Figure S7), the SiNW sensor achieved comparable temperature detection accuracy and exhibited significantly faster response times. Furthermore, the sensors were tested for continuous skin temperature monitoring by placing them on human skin. As shown in Figure 5i, when attached to the skin, the detected currents gradually increased and stabilized at a value corresponding to a temperature of 30.7 °C. Interestingly, upon detaching the sensor from the skin, the current returned to its initial value within 6 s.

Given that breathing and blowing actions also affect airflow and humidity conditions, we conducted a simple experiment to study their impact on temperature sensing. The thin poly(methyl methacrylate) (PMMA) layers were spin-coated onto the sensors, and hot steam (~40 °C) was delivered onto the channel area using a humidifier. The thin PMMA films were intended to shield the sensitive area from air disturbances and steam. The results shown in Figures S8a and S8b indicated that the voltage signals in the sensors with and without the PMMA film were very similar, with the $\Delta I/I_0 \sim 1.5\%$, demonstrating that the influence of air disturbances or humidity during breathing monitoring can be excluded. Additionally, the SiNW sensors exhibited stable temperature sensing performance over a period of 2 weeks, as shown in Figure S9. When placed in a normal ambient environment without protection, the sensitivity decreased from 6.0% to 4.5%, indicating a moderate reduction but overall stability.

https://doi.org/10.1021/acs.nanolett.4c05235
Nano Lett. 2025, 25, 4196−4203

Recent advancements in continuous temperature sensors based on inorganic materials and organic materials are summarized in Table S1. Most thermosensitive materials are commonly used as coating or incorporated with other materials to form sensitive films on substrates, with typical TCR values less than 1.6%/°C. Metallic oxide films, such as NiO and MnCoNiO, exhibit an excellent TCR value (up to 9.2%/°C), while they have a large film thickness of ∼30 μm. Therefore, compared with the sensitive film sensors and NW sensors in previous studies, our self-aligned SiNW thermoreceptors demonstrate an excellent TCR of 1.8%/°C and are compatible with mature Si technology for high-density device integration, making them potentially applicable for continuous and rapid monitoring and mapping of temperature variations.

In summary, we developed artificial thermoreceptor sensors using IPSLS SiNW arrays as sensitive channels for continuous and rapid temperature monitoring. Annealing at 450 °C significantly enhanced their conductivity and improved the metal electrode contact, enabling the fabricated sensors to exhibit linear thermal responses to temperature variations and an excellent TCR of −1.8%/°C. The sensors demonstrated a unique capability for continuous temperature monitoring and spatial analysis of thermal sources. The superior sensing performance of the SiNW sensors can be attributed to the changes of conductive surface defects induced by low-temperature annealing, while the high-temperature annealing may lead to a significant diffuseness of the dissolved In atoms from the SiNW cores into the outer SiO_2 shell. The sensors have comparable temperature detection accuracy and excellent environmental adaptability and stability, enabling the continuous monitoring of human breathing and blowing activities, with a fast response time of ∼0.2 s and recovery time of ∼1 s. Therefore, this work demonstrates that the self-aligned IPSLS SiNW arrays provide solid sensitive materials for high-performance artificial temperature sensors, suitable for applications in human disease diagnosis and monitoring.

■ ASSOCIATED CONTENT

Supporting Information

The Supporting Information is available free of charge at https://pubs.acs.org/doi/10.1021/acs.nanolett.4c05235.

Experimental Section; diameter distribution of SiNWs; uniformity testing of the SiNW sensors; photoresponse of annealed SiNW sensors under LED light illumination; current−voltage curves of the sensors fabricated using SiNW annealed at 650 and 850 °C; $\ln(1/R)$ vs $1/kT$ curves for SiNW annealed at various temperatures; TEM image and elemental distribution of FIB-etched SiNW (annealing at 450 °C); environmental adaptability of the sensors; temperature sensing performance with or without PMMA coating; long-term stability measurement of the SiNW temperature sensor; comparison of artificial SiNW thermoreceptor with other temperature sensors reported in the literature (PDF)

■ AUTHOR INFORMATION

Corresponding Authors

Jianmei Chen − *Institute of Translational Medicine, Medical College, Yangzhou University, Yangzhou 225009, P. R. China;* orcid.org/0000-0002-0646-5234; Email: cjm@yzu.edu.cn

Linwei Yu − *School of Electronic Science and Engineering/National Laboratory of Solid-State Microstructures, Nanjing University, Nanjing 210023, P. R. China;* orcid.org/0000-0002-0801-5210; Email: yulinwei@nju.edu.cn

Authors

Zongguang Liu − *Microelectronics Industry Research Institute, College of Physics Science and Technology, Yangzhou University, Yangzhou 225009, P. R. China;* orcid.org/0000-0003-4141-7462

Rongrong Yuan − *School of Electronic Science and Engineering/National Laboratory of Solid-State Microstructures, Nanjing University, Nanjing 210023, P. R. China*

Shuyi Wang − *School of Electronic Science and Engineering/National Laboratory of Solid-State Microstructures, Nanjing University, Nanjing 210023, P. R. China*

Wei Liao − *School of Electronic Science and Engineering/National Laboratory of Solid-State Microstructures, Nanjing University, Nanjing 210023, P. R. China;* orcid.org/0009-0006-8804-9395

Lei Yan − *School of Electronic Science and Engineering/National Laboratory of Solid-State Microstructures, Nanjing University, Nanjing 210023, P. R. China;* orcid.org/0000-0002-6776-2400

Ruijin Hu − *Microelectronics Industry Research Institute, College of Physics Science and Technology, Yangzhou University, Yangzhou 225009, P. R. China;* orcid.org/0009-0006-5973-6954

Complete contact information is available at: https://pubs.acs.org/10.1021/acs.nanolett.4c05235

Notes

The authors declare no competing financial interest.

■ ACKNOWLEDGMENTS

The authors acknowledge the financial support received from the National Natural Science Foundation of China under Grant No. 62104100, Educational Commission Key (Key grant) Project of Anhui Province of China under No. 2024AH040204, National Key Research Program of China under No. 92164201, and National Natural Science Foundation of China for Distinguished Young Scholars under No. 62325403.

■ REFERENCES

(1) Li, S.; Zhang, Y.; Wang, Y.; Xia, K.; Yin, Z.; Wang, H.; Zhang, M.; Liang, X.; Lu, H.; Zhu, M.; et al. Physical sensors for skin-inspired electronics. *InfoMat* **2020**, *2* (1), 184−211.

(2) Li, Q.; Zhang, L. N.; Tao, X. M.; Ding, X. Review of flexible temperature sensing networks for wearable physiological monitoring. *Adv. Healthcare Mater.* **2017**, *6* (12), No. 1601371.

(3) Guan, W.-j.; Ni, Z.-y.; Hu, Y.; Liang, W.-h.; Ou, C.-q.; He, J.-x.; Liu, L.; Shan, H.; Lei, C.-l.; Hui, D. S.; et al. Clinical characteristics of coronavirus disease 2019 in China. *New England journal of medicine* **2020**, *382* (18), 1708−1720.

(4) Nagai, M.; Moriyama, M.; Ishii, C.; Mori, H.; Watanabe, H.; Nakahara, T.; Yamada, T.; Ishikawa, D.; Ishikawa, T.; Hirayama, A.; et al. High body temperature increases gut microbiota-dependent host resistance to influenza A virus and SARS-CoV-2 infection. *Nat. Commun.* **2023**, *14* (1), 3863.

(5) Liu, Q.; Tai, H.; Yuan, Z.; Zhou, Y.; Su, Y.; Jiang, Y. A high-performances flexible temperature sensor composed of polyethyle-

neimine/reduced graphene oxide bilayer for real-time monitoring. *Advanced Materials Technologies* **2019**, *4* (3), No. 1800594.
(6) Trung, T. Q.; Ramasundaram, S.; Hwang, B. U.; Lee, N. E. An all-elastomeric transparent and stretchable temperature sensor for body-attachable wearable electronics. *Advanced materials* **2016**, *28* (3), 502−509.
(7) Harada, S.; Kanao, K.; Yamamoto, Y.; Arie, T.; Akita, S.; Takei, K. Fully printed flexible fingerprint-like three-axis tactile and slip force and temperature sensors for artificial skin. *ACS Nano* **2014**, *8* (12), 12851−12857.
(8) Shin, J.; Jeong, B.; Kim, J.; Nam, V. B.; Yoon, Y.; Jung, J.; Hong, S.; Lee, H.; Eom, H.; Yeo, J.; Choi, J.; Lee, D.; Ko, S. H. Sensitive Wearable Temperature Sensor with Seamless Monolithic Integration. *Adv. Mater.* **2020**, *32* (2), No. e1905527.
(9) Ge, G.; Lu, Y.; Qu, X.; Zhao, W.; Ren, Y.; Wang, W.; Wang, Q.; Huang, W.; Dong, X. Muscle-inspired self-healing hydrogels for strain and temperature sensor. *ACS Nano* **2020**, *14* (1), 218−228.
(10) Ban, J.; Lu, Y.; Lu, J.; Jia, K.; Luo, M.; Zhou, Y.; Wang, D.; Piao, L. Highly sensitive stretchable fiber-based temperature sensor enhanced by surface-chemically modified silver nanowires. *Chemical Engineering Journal* **2024**, *482*, No. 148772.
(11) Yin, R.; Yang, S.; Li, Q.; Zhang, S.; Liu, H.; Han, J.; Liu, C.; Shen, C. Flexible conductive Ag nanowire/cellulose nanofibril hybrid nanopaper for strain and temperature sensing applications. *Science Bulletin* **2020**, *65* (11), 899−908.
(12) Cui, Z.; Poblete, F. R.; Zhu, Y. Tailoring the temperature coefficient of resistance of silver nanowire nanocomposites and their application as stretchable temperature sensors. *ACS Appl. Mater. Interfaces* **2019**, *11* (19), 17836−17842.
(13) Li, S.; Liu, D.; Tian, N.; Liang, Y.; Gao, C.; Wang, S.; Zhang, Y. High-performance temperature sensor based on silver nanowires. *Materials Today Communications* **2019**, *20*, No. 100546.
(14) Ma, X.; Wang, C.; Wei, R.; He, J.; Li, J.; Liu, X.; Huang, F.; Ge, S.; Tao, J.; Yuan, Z.; et al. Bimodal tactile sensor without signal fusion for user-interactive applications. *ACS Nano* **2022**, *16* (2), 2789−2797.
(15) Fan, X.; Stott, N. E.; Zeng, J.; Li, Y.; Ouyang, J.; Chu, L.; Song, W. PEDOT: PSS materials for optoelectronics, thermoelectrics, and flexible and stretchable electronics. *Journal of Materials Chemistry A* **2023**, *11* (35), 18561−18591.
(16) Yu, Y.; Peng, S.; Blanloeuil, P.; Wu, S.; Wang, C. H. Wearable Temperature Sensors with Enhanced Sensitivity by Engineering Microcrack Morphology in PEDOT:PSS−PDMS Sensors. *ACS Appl. Mater. Interfaces* **2020**, *12* (32), 36578−36588.
(17) Wu, Z.; Ding, H.; Tao, K.; Wei, Y.; Gui, X.; Shi, W.; Xie, X.; Wu, J. Ultrasensitive, stretchable, and fast-response temperature sensors based on hydrogel films for wearable applications. *ACS Appl. Mater. Interfaces* **2021**, *13* (18), 21854−21864.
(18) Zhang, J.; Yan, K.; Huang, J.; Sun, X.; Li, J.; Cheng, Y.; Sun, Y.; Shi, Y.; Pan, L. Mechanically Robust, Flexible, Fast Responding Temperature Sensor and High-Resolution Array with Ionically Conductive Double Cross-Linked Hydrogel. *Adv. Funct. Mater.* **2024**, *34* (21), No. 2314433.
(19) Li, Y.; Li, D.; Wang, J.; Ye, T.; Li, Q.; Li, L.; Gao, R.; Wang, Y.; Ren, J.; Li, F.; et al. A Temperature-Sensing Hydrogel Coating on The Medical Catheter. *Adv. Funct. Mater.* **2024**, *34* (10), No. 2310260.
(20) Neto, J.; Chirila, R.; Dahiya, A. S.; Christou, A.; Shakthivel, D.; Dahiya, R. Skin-Inspired Thermoreceptors-Based Electronic Skin for Biomimicking Thermal Pain Reflexes. *Adv. Sci. (Weinh)* **2022**, *9* (27), No. e2201525.
(21) Yu, L.; Alet, P.-J.; Picardi, G.; Roca i Cabarrocas, P. An In-plane solid-liquid-solid growth mode for self-avoiding lateral silicon nanowires. *Phys. Rev. Lett.* **2009**, *102* (12), No. 125501.
(22) Xue, Z.; Sun, M.; Dong, T.; Tang, Z.; Zhao, Y.; Wang, J.; Wei, X.; Yu, L.; Chen, Q.; Xu, J.; Shi, Y.; Chen, K.; Roca i Cabarrocas, P. Deterministic line-shape programming of silicon nanowires for extremely stretchable springs and electronics. *Nano Lett.* **2017**, *17* (12), 7638−7646.
(23) Liu, Z.; Yan, J.; Ma, H.; Hu, T.; Wang, J.; Shi, Y.; Xu, J.; Chen, K.; Yu, L. Ab initio design, shaping, and assembly of free-standing silicon nanoprobes. *Nano Lett.* **2021**, *21* (7), 2773−2779.
(24) Sun, Y.; Dong, T.; Yu, L.; Xu, J.; Chen, K. Planar growth, integration, and applications of semiconducting nanowires. *Adv. Mater.* **2020**, *32* (27), No. 1903945.
(25) Yan, J.; Zhang, Y.; Liu, Z.; Wang, J.; Xu, J.; Yu, L. Ultracompact single-nanowire-morphed grippers driven by vectorial Lorentz forces for dexterous robotic manipulations. *Nat. Commun.* **2023**, *14* (1), 3786.
(26) Xu, M.; Wang, J.; Xue, Z.; Wang, J.; Feng, P.; Yu, L.; Xu, J.; Shi, Y.; Chen, K.; Roca, I. C. P. High performance transparent in-plane silicon nanowire Fin-TFTs via a robust nano-droplet-scanning crystallization dynamics. *Nanoscale* **2017**, *9* (29), 10350−10357.
(27) Yin, H.; Yang, H.; Xu, S.; Pan, D.; Xu, J.; Chen, K.; Yu, L. High Performance Si Nanowire TFTs With Ultrahigh on/off Current Ratio and Steep Subthreshold Swing. *IEEE Electron Device Lett.* **2020**, *41* (1), 46−49.
(28) Dong, T.; Sun, Y.; Zhu, Z.; Wu, X.; Wang, J.; Shi, Y.; Xu, J.; Chen, K.; Yu, L. Monolithic Integration of Silicon Nanowire Networks as a Soft Wafer for Highly Stretchable and Transparent Electronics. *Nano Lett.* **2019**, *19* (9), 6235−6243.
(29) Liu, Z.; Yan, J.; Ma, H.; Hu, T.; Wang, J.; Shi, Y.; Xu, J.; Chen, K.; Yu, L. Ab Initio Design, Shaping, and Assembly of Free-Standing Silicon Nanoprobes. *Nano Lett.* **2021**, *21* (7), 2773−2779.
(30) Norton, P.; Brandt, J. Temperature coefficient of resistance for p-and n-type silicon. *Solid-state electronics* **1978**, *21* (7), 969−974.
(31) Zhang, B.-C.; Jie, J.-S.; Shao, Z.-B.; Huang, S.-Y.; He, L.; Zhang, X.-H. One-step growth of large-area silicon nanowire fabrics for high-performance multifunctional wearable sensors. *Nano Research* **2019**, *12* (11), 2723−2728.
(32) Wang, C.-P.; Liu, C.-W.; Gau, C. In *Silicon nanowire temperature sensor and its characteristic, 2011 6th IEEE International Conference on Nano/Micro Engineered and Molecular Systems*; IEEE: 2011; pp 630−633.
(33) Song, X. P.; Wu, L.; Liang, Y. F.; Liu, Z. G.; Wang, J. Z.; Xu, J.; Chen, K. J.; Yu, L. W. High-Performance Transparent Silicon Nanowire Thin Film Transistors Integrated on Glass Substrates via a Room Temperature Solution Passivation. *Advanced Electronic Materials* **2023**, *9* (4), No. 2201236.
(34) Liang, L.; Wu, L.; Liao, W.; Qian, W.; Zhang, Y.; Hu, R.; Wang, J.; Yu, L. Performance improvement of planar silicon nanowire field effect transistors via catalyst atom doping control. *J. Alloys Compd.* **2024**, *1001*, No. 175189.
(35) Islam, M. R.; Afroj, S.; Yin, J.; Novoselov, K. S.; Chen, J.; Karim, N. Advances in Printed Electronic Textiles. *Advanced Science* **2024**, *11* (6), No. 2304140.
(36) Hua, Q.; Sun, J.; Liu, H.; Bao, R.; Yu, R.; Zhai, J.; Pan, C.; Wang, Z. L. Skin-inspired highly stretchable and conformable matrix networks for multifunctional sensing. *Nat. Commun.* **2018**, *9* (1), 244.
(37) Mansour, E.; Vishinkin, R.; Rihet, S.; Saliba, W.; Fish, F.; Sarfati, P.; Haick, H. Measurement of temperature and relative humidity in exhaled breath. *Sens. Actuators, B* **2020**, *304*, No. 127371.

https://doi.org/10.1021/acs.nanolett.4c05235
Nano Lett. 2025, 25, 4196−4203